Acta Crystallographica Section A
Foundations of Crystallography
ISSN 0108-7673

Received 18 October 2002
Accepted 3 January 2003

A holographic approach to point defect structure determination in inorganic crystals: Er-doped Sc_2O_3

Karin Anduleit[a]* and Gerhard Materlik[a,b]

[a]HASYLAB at DESY, Notkestrasse 85, 22607 Hamburg, Germany, and [b]Diamond Light Source Ltd, Rutherford Appleton Laboratory, Chilton, Didcot, Oxon OX11 0QX, England. Correspondence e-mail: karin.anduleit@desy.de

A holographic approach to the analysis of a Bragg scattering pattern has been described by Szöke [*Acta Cryst.* (1993), A**49**, 853–866]. The combination of crystallographic procedures and holographic interpretation allows reconstruction of an unknown part of the crystalline structure model-free if the other part of the structure is known. By introducing the concept of an average crystal, this approach is extended to point defect structures in inorganic crystals. In this case, the host lattice is well known while the defect structure is regarded as the unknown part. To demonstrate the feasibility of this approach, an Sc_2O_3 sample doped with Er at low concentration has been studied. An additional electron density has been observed, which can be interpreted as an interstitial Er position.

1. Introduction

The idea of holography in the range of X-ray wavelengths has been proposed by Gábor (1948) and later extended by Szöke (1986). The advantages are clear: holography can reveal a three-dimensional image of the specimen without using a model. The holographic principle is simple: part of a well known reference wave is scattered by the unknown object. This scattered wave interferes with the reference wave causing an intensity modulation which is then recorded in the far field outside the sample. With the knowledge of the reference wave, phase information is conserved in this modulation. While in the visible light range the object is reconstructed by illuminating the hologram again with a replica of the reference wave, this is done numerically for X-rays. In terms of crystallography: as in a holographic image, the phase information is conserved, the object can be reconstructed without refinement. Atomic resolution holography as has been proposed by Szöke (1986) uses the fluorescence of an atom as a reference wave to image its surrounding.

As this method is element specific and can image the surrounding of each atom of interest, it would be the ideal technique to study point defects in inorganic crystals. Usually these defects are randomly spread objects, *e.g.* dopants which can be built into the host crystal either on lattice sites or on interstitial positions. In any case, they will influence their surroundings because their physical properties differ from those of the regular atoms. Unfortunately, as the concentration of these defects is often of the order of 0.1–10%, atomic resolution X-ray fluorescence holography is so far not sensitive enough to study their influence on the host crystal, their fluorescence intensity is too small to record a hologram in reasonable time.

The most common approach to determine the dopant positions is to measure Bragg reflections, which ensures a maximum amount of signal, and to refine a preliminary model to these data. In some cases, it will also be possible to study diffuse scattering as the point defects are not periodically ordered. Both approaches depend on a good model while it is often desirable to use a model-free approach like in holography.

Thus, Szöke (1993) proposed a new approach that combines the advantages of both methods. The Bragg scattering pattern as a whole is interpreted as a hologram and is reconstructed model-free, where the known part of the crystal creates the reference wave. This approach has been applied in the program package *EDEN* (Somoza *et al.*, 1995), written originally for protein crystallography by H. Szöke. In this paper, we show that it is also very suitable for studying point defect structures.

To demonstrate the feasibility of this approach, the structure of erbium ($\sim$0.4%) in Sc_2O_3 has been studied. This object is of great interest: chemically, erbium is assumed to replace scandium but with an ionic radius 20% larger than Sc it will have to distort its surrounding. Additionally, spectroscopic measurements, carried out at the Institute of Laser Physics at the University of Hamburg, indicate that the atomic arrangement in this material might be even more complicated, as pointed out in Peters *et al.* (1998).

2. The method

As described in Szöke (1993), an X-ray diffraction pattern of a partially known material can also be seen as a hologram. The

principles of this approach will be presented here shortly, for a more detailed explanation please refer to the literature.

An incoming monochromatic plane wave of X-rays is scattered by the host crystal. Owing to its long-range periodic structure, high intensity is only observed in very discrete spots – the Bragg reflections. They occur whenever the Bragg condition is fulfilled and the scattering from every unit cell adds up coherently while all waves average out to zero in between the Bragg spots.

In our case, the host lattice is known. The wave scattered by this perfect crystal can be calculated for every scattering vector **H** being proportional to

$$R = \sum \int_{\mathrm{UC}} \rho_{\mathrm{known}}(\mathbf{r}) \exp(2\pi i \mathbf{h} \cdot \mathbf{r}) \, \mathrm{d}^3 r. \quad (1)$$

The integration is carried out over the unit cell of the host crystal and summed over the whole crystal. This is the well known structure factor for the known undisturbed structure – we will call this the reference wave.

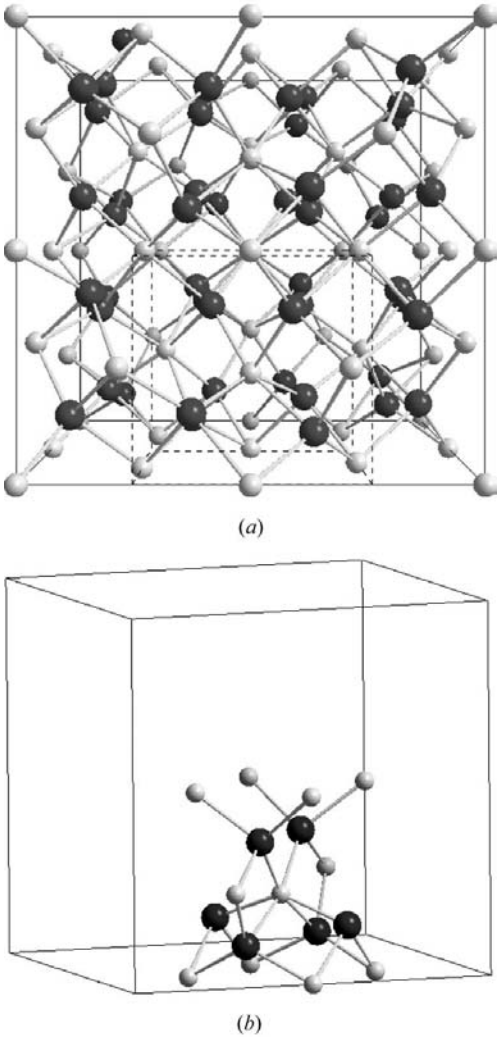

Figure 1
The Sc_2O_3 structure. For a better orientation, a part of the unit cell is shown below. Dark spheres indicate oxygen, lighter spheres scandium.

Bragg scattering always averages over the entire crystal. Therefore, the electron-density distribution that can be seen as producing the (Bragg) scattering pattern is the average crystal (Cowley, 1981). In the case that a dopant is present, the unit cell will look slightly different, *e.g.* atoms are displaced. For low concentrations of defects, we can assume that they do not distort the structure over a range that is much larger than a unit cell. Therefore, we assume that this defect structure can be understood as an electron-density distribution in the unit cell which differs slightly from that of the undisturbed host crystal. We call this distorted 'unit cell' that contains the defect structure ρ_{unknown}. The electron density of the average crystal will be the sum of both undisturbed host lattice and defect structure, weighted with the probability w of their appearance:

$$\rho_{\mathrm{av}}(\mathbf{r}) = (1 - w)\rho_{\mathrm{known}}(\mathbf{r}) + w\rho_{\mathrm{unknown}}(\mathbf{r}). \quad (2)$$

The wave scattered at the unknown part of the crystal – the dopants and their surroundings – can be formally written in analogy to (1) as

$$O = \sum \int_{\mathrm{UC}} \rho_{\mathrm{unknown}}(\mathbf{r}) \exp(2\pi i \mathbf{h} \cdot \mathbf{r}) \, \mathrm{d}^3 r. \quad (3)$$

We call it the object wave, as the underlying density distribution is the object we are interested in.

The dopant structure is therefore understood as a different unit cell with the same size but different electron-density distribution. The dopants occupy a similar site in each unit cell in which they are present. These unit cells are therefore similar but their arrangement is non-periodic as the dopant is not present in every unit cell.

This approach is closely related to time-resolved X-ray diffraction (Szöke, 1999), where a structural change of the molecule in the crystal is induced *e.g.* by a laser pulse. This structural change does not affect every molecule but only a certain number of randomly spread unit cells. The structure probed with the X-ray pulse then consists of a spatial ordered lattice of randomly distorted and undistorted unit cells.

The intensity for a scattering vector **h** is then given by:

$$\begin{aligned} I(\theta_B) &\propto |F(\mathbf{h})|^2 \\ &= |R(\mathbf{h}) + O(\mathbf{h})|^2 \quad (4) \\ &= |R(\mathbf{h})|^2 + R(\mathbf{h})O^*(\mathbf{h}) + R^*(\mathbf{h})O(\mathbf{h}) + |O(\mathbf{h})|^2. \quad (5) \end{aligned}$$

The squared self-interference terms are pure intensity terms while the interference terms still contain phase information. Note that the deformed unit cells do not have to have their own translational periodicity. It is useful to think about how the 'solution' of this intensity pattern will look. We know that our structure is periodic in wide ranges (the concentration of distortions is low), therefore we will observe a very clear Bragg pattern. This periodicity is broken in some places by the randomly spread dopants. The wave scattered by these objects interferes with the reference wave causing a small modulation on the perfect Bragg pattern, which is described by the interference terms. The self-interference term $|O(\mathbf{h})|^2$ will be negligibly small.

Subtracting the known host crystal $\rho_{\rm known}$ from this $\rho_{\rm av}$, the remaining electron-density distribution will be essentially the structure of the defects.

The program package *EDEN* (Somoza *et al.*, 1995) provides a powerful tool to solve (4). The unknown electron density is decomposed into a set of Gaussian basis functions in real space, which are placed on a regular grid in the unit cell. The grid spacing Δr corresponds to the resolution of the measured data and the width of the Gauss functions is fixed relative to this spacing by the fraction η while their height is a free parameter n_p.

$$\rho_{\rm unknown} \approx \rho_{\rm approx} = (\pi\eta\Delta r^2)^{-3/2} \sum_{p=1}^{P} n_p \exp\left(-\frac{(\mathbf{r}-\mathbf{r}_p)^2}{\eta\Delta r^2}\right). \quad (6)$$

Inserted into (4), this expression is transformed into a set of quadratic equations with as many unknowns as basis functions in the unit cell and as many equations as reflections have been measured. *EDEN* solves this equation in linearized form using a conjugate gradient solver and then iteratively adds up the newly recovered electron density to the reference structure. The algorithm is constrained by using the positivity of the electron density to stabilize convergence. Available symmetry information is also used to simplify the problem.

3. The material: Sc_2O_3

Sc_2O_3 is a material of interest in laser physics, like several other sesquioxides. The structure is shown in Fig. 1. It crystallizes in space group $Ia\bar{3}$ having a lattice constant of approximately 9.85 Å (Schleid & Meyer, 1989). With 16 formula units in the unit cell, three positions are observed: a general oxygen position 48(*e*) and two Sc positions, a high symmetry 8(*a*) and a lower symmety 24(*d*), located on the twofold axes. Apart from small dislocations of the 24(*d*) Sc atoms, the structure can be understood as eight f.c.c. lattices, formed by Sc. Each of these is surrounded by six oxygen atoms in the form of a strongly deformed octahedron or better a cube with two missing corners. This is described well in Pauling & Shappell (1930).

Sc_2O_3 can be doped with several rare earths, which are assumed to replace Sc as trivalent ions. Recently, there have been successful attempts to grow large crystals of high quality using a heat-exchanger method (Peters, 2001). The maximum dopant concentration of Er has been observed to be relatively low (∼0.4%). If Er is substituted for Sc, it is expected to distort its surrounding strongly because of its ionic radius ($r_{\rm Er}$ = 0.89 Å) being about 20% larger than that of Sc ($r_{\rm Sc}$ = 0.75 Å). In addition, the structure is relatively dense. In time-resolved emission measurements, the radiative lifetime of the Er $4S_{3/2}$ state has been observed to be drastically smaller for Er in Sc_2O_3 than for comparable compounds, *e.g.* $Er:Lu_2O_3$ and $Er:Y_2O_3$ (Peters *et al.*, 1998). This indicates that Er occupies a site of lower symmetry in Sc_2O_3 than in Lu_2O_3 or Y_2O_3. Therefore, there is a lot of indirect evidence that Er does not replace Sc and it is of great interest to understand how Er is incorporated into the host crystal.

4. Experimental

Two Sc_2O_3 crystals have been studied: one undoped, the other doped with Er (∼0.4%). This provides us with the opportunity to compare them directly. The crystals (usually of cm size) were split into fragments of approximately 300 µm diameter. Data were collected in a common Bragg scattering experiment, using a four-circle diffractometer at beamline D3 at HASYLAB. An energy of 31 keV has been chosen using an Si(111) double-crystal monochromator. At this energy, the influence of absorption can be neglected. Intensities of reflections in 1/8 of the reciprocal space have been measured in ω-scan geometry. No hint of a superstructure has been found. The data sets were relatively large, especially for the doped crystal, where reflections have been measured up to $\sin\theta/\lambda = 0.57$ Å^{-1}. The data have been corrected for drift. To fit into the equation system to be solved, the data additionally have been scaled to absolute values and the resolution was decreased to fit the desired grid spacing of 0.125 Å. This is done by introducing an artificial Debye–Waller factor which has the effect of smearing out the electron density in real space (Somoza *et al.*, 1995). In addition to that, it was necessary to correct for extinction effects. For this task, a formula similar to that proposed by Larson (1970) has been used:

$$|F_{\rm obs\,ext}| = |F_{\rm obs}|\left[1 + \frac{0.001 x F_{\rm calc}^2 \lambda^3}{\sin(2\theta_B)}\right]^{1/4}. \quad (7)$$

Here, x is the extinction factor, θ_B the Bragg angle and λ the wavelength. For both data sets, the (well known) Sc_2O_3 structure serves as reference wave, as has been described by (1). Since this contribution of the host crystal strongly dominates the structure factors, the reference wave gives us the calculated structure factors in (7) for the extinction correction $R \approx F_{\rm calc}$. This can be done without noticeable inaccuracy. The value of the extinction factor was found iteratively using an individual weighting for each reflection. In that way, the reflections which were mostly affected by extinction were systematically under-weighted in the first iterations of the algorithm.

5. The results

The calculations of *EDEN* converged well, leading to a crystallographic R factor of 2% for the doped and 3% for the undoped data set. Comparing the result for the undoped crystal with the calculated model structure, the agreement was excellent, which proves that *EDEN* delivers the correct solution for these samples.

When calculating the difference between the two solutions $\rho_{\rm doped}(\mathbf{r}) - \rho_{\rm undoped}(\mathbf{r})$, essentially the influence of the defect structure remains. It has been found that additional peaks in the electron density appear, which are present in the doped structure but not in the undoped structure. These peaks are

very small, but subtracting the density map of the undoped crystal from the density map of the doped crystal shows them clearly. This is shown in Fig. 2 for a part of the unit cell, cut perpendicular to the [001] direction at $z = 0.075$. The peaks appear distinctly displaced from the Sc position. They can be identified even more clearly in the weighted difference,

$$\frac{\rho_{\rm doped}(\mathbf{r}) - \rho_{\rm undoped}(\mathbf{r})}{\rho_{\rm undoped}(\mathbf{r})}.$$

Their position can be identified as 48(*e*) (0.15, 0.11, 0.06) with an accuracy of ±0.0125. The result is shown in Fig. 3 and in schematic illustration in Fig. 4 for a cube, cut from the unit cell in ($0.25 \le x < 0.75$, $0 \le y < 0.5$, $0 \le z < 0.5$) which corresponds to 1/8 of the unit-cell volume. Their site can be understood as occupying the two corners of the oxygen cube that are empty in the undisturbed structure (see §3). In each of these corners, three symmetry-equivalent positions can be distinguished, each of them situated very close to one of the neighbouring oxygen atoms.

This observation can be explained as follows: having a larger ionic radius than Sc, Er is too large to replace Sc atoms without distorting the lattice heavily. Therefore it occupies a different position, which we observed as additional peaks. Remembering that during the growth process, depending on

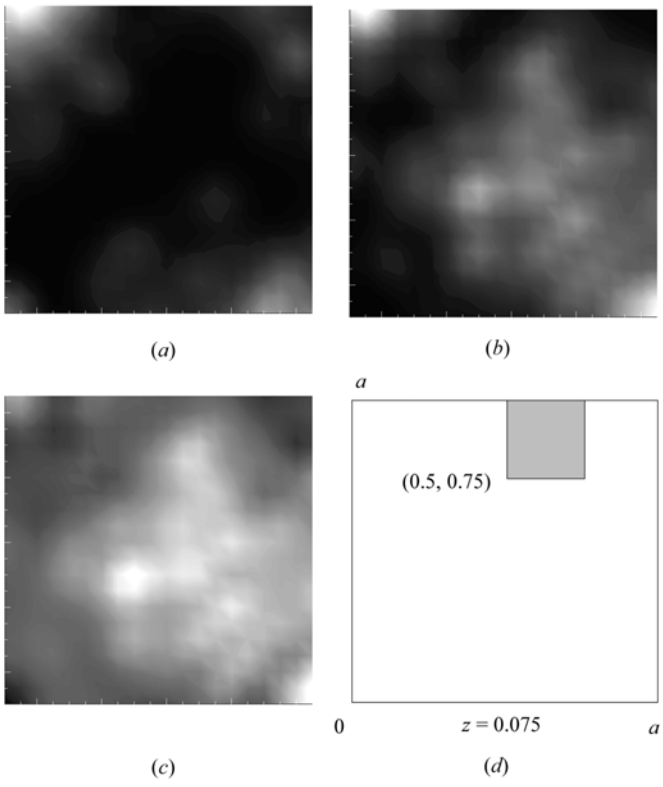

Figure 2
A cut through the electron-density map at $z = 0.075$ perpendicular to the [001] direction. In (*d*) the region shown in (*a*)–(*c*) is marked. Light colours indicate regions of high electron density. (*a*) Reconstructed electron density of the undoped crystal, (*b*) the same cutout from the doped crystal and (*c*) the difference between the two clearly shows an additional electron density.

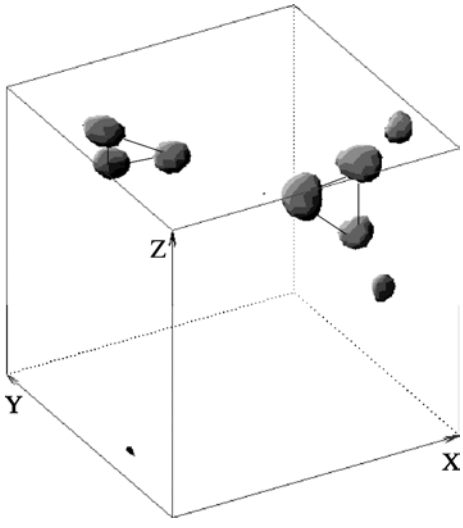

Figure 3
The additional peaks in part of the unit cell appear clearly in the weighted electron density, which is here convoluted with a Gaussian function (σ = 0.25 Å, cut-off level 50% of maximum) for better visibility. Shown here is the same part of the unit cell as in Figs. 1 and 4.

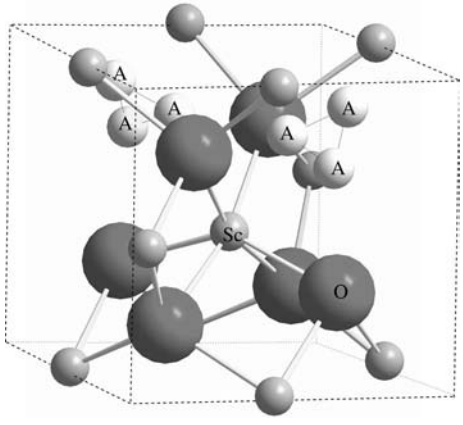

Figure 4
The position of the additional peaks (A) in part of the unit cell, for further details refer to text.

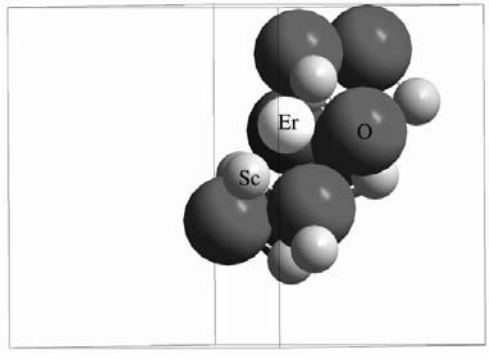

Figure 5
An erbium atom (white) surrounded by its neighbouring oxygen atoms. The radii of the atoms are shown in correct relations.

the temperature, a certain amount of sites remain vacant (Vainshtein, 1996), this suggests that Er, occupying the position described here, is always coupled with an oxygen vacancy. Assuming that an oxygen atom is missing and that the remaining atoms in the same plane have the freedom to relax to a limited extent, the space is large enough to contain an Er atom. Allowing a relaxation of about 0.2 Å, which is approximately twice our resolution limit, all neighbouring O atoms fulfil the requirement of an Er—O interatomic distance of about 2.3 Å. This is illustrated in Fig. 5. These oxygen relaxations cannot be observed directly as the charge density in these relaxed positions is not only very weak but the 'relaxation distance' we assumed is also smaller than the dislocation of the oxygen position itself owing to its artificial (see §4) and thermal Debye–Waller factor, which can be estimated from the spatial distribution. A slightly asymmetric electron-density distribution for the oxygen atoms would support this explanation. Indeed this has been observed in the reconstruction with *EDEN*.

To further fortify this explanation, some estimations about the concentrations of Er and O vacancies can be made. The approximate amount of vacancies can be estimated from the equilibrium concentration (Vainshtein, 1996). It is likely that the concentration of vacancies is most likely higher than the equilibrium concentration because of the rapid cooling and can be of the order of magnitude of 10^{-4}–10^{-3}. Calculating the dopant concentration from the electron density leads to an Er concentration of 0.3% at maximum, which is consistent and confirms our explanation. It also has to be stressed that *EDEN* can deliver absolute values for the dopant concentration that agree well with our concentration of ∼0.4%. The lower symmetry of the site can also explain the observations made in measurements of the radiative lifetime of the Er $4S_{3/2}$ state (Peters, 2001). It is also possible that Er forms a pair with one Er atom replacing the neighbouring Sc atom. This cannot be excluded as the electron density in the Sc positions of the doped crystal differs slightly from that of the undoped crystal.

6. Summary

Using a holographic approach, the dopant structure of Er in Sc_2O_3 has been studied. A small modulation of a Bragg scattering pattern, caused by the dopant and its surroundings, has been interpreted as a hologram. The underlying electron-density distribution has been reconstructed using the software package *EDEN*, proving its feasibility to reconstruct small changes in the electron density by using the interference terms.

Comparing the Er-doped structure of Sc_2O_3 with the undoped structure, additional peaks have been observed. They can be interpreted as an interstitial Er position, coupled with an oxygen vacancy. The observed electron density is consistent with the dopant concentration. The proposed model can explain the results of spectroscopic measurements.

The holographic approach is certainly not meant to replace other methods of studying defect structures but it provides us with an approximate image of the average crystal which can then be interpreted and used to construct a model for further structural investigations. The great advantage of this method is its independence of complicated measurement techniques and its model-free approach.

The crystals that were mentioned here have been grown at the Institute of Laser Physics, University of Hamburg. The authors thank V. Peters, K. Petermann and G. Huber from this Institute for providing the crystals and for fruitful discussions. We also thank H. and A. Szöke for the opportunity to use *EDEN* and H.-G. Krane for his help with the experiment.

References

Gábor, D. (1948). *Nature (London)*, **161**, 777.
Cowley, J. M. (1981). *Diffraction Physics*, 2nd ed. Amsterdam: North-Holland.
Larson, A. C. (1970). *Crystallographic Computing*, edited by F. R. Ahmed & C. P. Huber, pp. 291–294. Copenhagen: Munksgaard.
Pauling, L. & Shappell, M. D. (1930). *Z. Kristallogr.* **75**, 128–142.
Peters, V. (2001). PhD thesis, Universität Hamburg, Germany.
Peters, V., Fornasiero, L., Mix, E., Diening, A., Petermann, K. & Huber, G. (1998). In Proceedings CLEO-Europe, Glasgow, United Kingdom, technical digest CFF10.
Schleid, T. & Meyer, G. (1989). *J. Less-Common Met.* **149**, 73–80.
Somoza, J. R., Szöke, H., Goodman, D. M., Beran, P., Truckses, D., Kim, S.-H. & Szöke, A. (1995). *Acta Cryst.* A**51**, 691–703.
Szöke, A. (1986). In *Short Wavelength Coherent Radiation: Generation and Applications*, edited by D. T. Attwood & J. Bokor, No. 147 in *AIP Conf. Proc.*, pp. 361–367. New York: American Institute of Physics.
Szöke, A. (1993). *Acta Cryst.* A**49**, 853–866.
Szöke, A. (1999). *Chem. Phys. Lett.* **313**, 777–788.
Vainshtein, B. K. (1996). *Structure of Crystals.* Berlin: Springer.